MICROCOPY RESOLUTION TEST CHART

NATIONAL BUREAU OF STANDARDS-1963-A
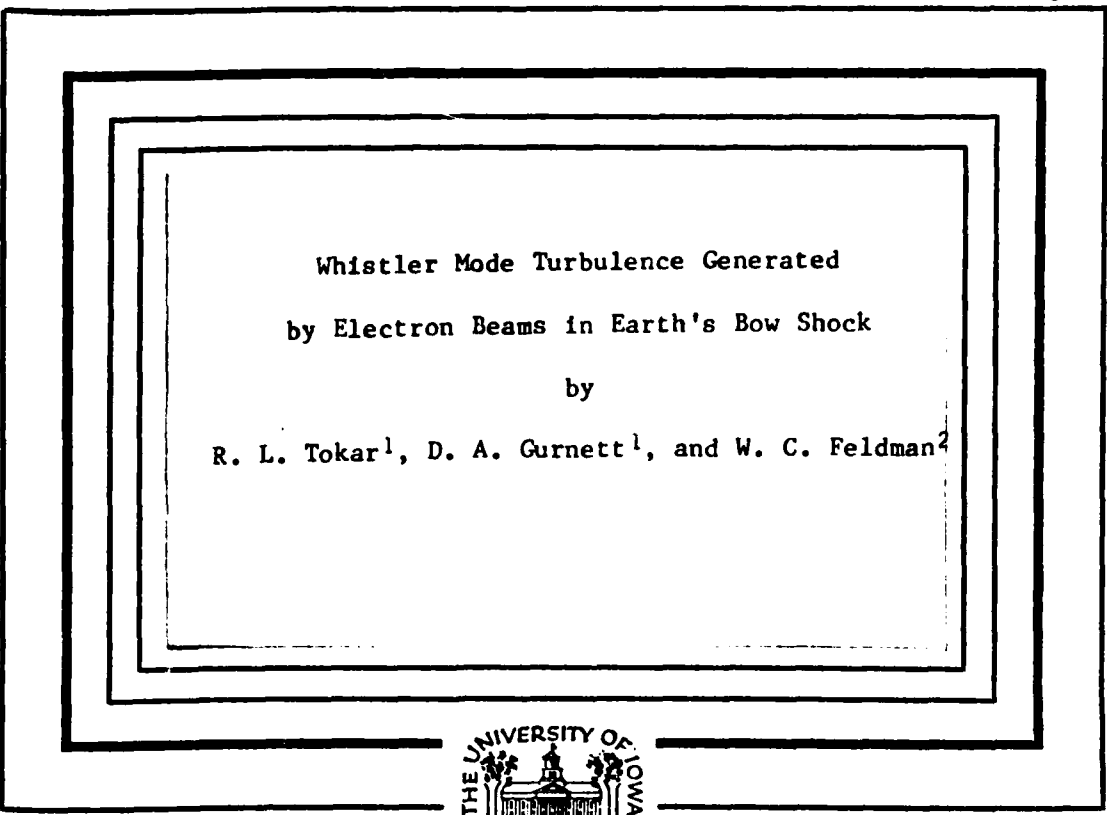
Whistler Mode Turbulence Generated

by Electron Beams in Earth's Bow Shock

by

R. L. Tokar[1], D. A. Gurnett[1], and W. C. Feldman[2]

THE UNIVERSITY OF IOWA
FOUNDED 1847

DTIC
ELECTE
NOV 2 1983
D

Department of Physics and Astronomy

THE UNIVERSITY OF IOWA

Iowa City, Iowa   52242

83 11 01 015

Whistler Mode Turbulence Generated

by Electron Beams in Earth's Bow Shock

by

R. L. Tokar[1], D. A. Gurnett[1], and W. C. Feldman[2]

May 1983

[1] Department of Physics and Astronomy
The University of Iowa
Iowa City, IA   52242

[2] Los Alamos Scientific Laboratory
Los Alamos, NM   87545

To appear in J. Geophys. Res.

REPORT DOCUMENTATION PAGE		READ INSTRUCTIONS BEFORE COMPLETING FORM
1. REPORT NUMBER U. of Iowa 83-17	2. GOVT ACCESSION NO. AD-A134274	3. RECIPIENT'S CATALOG NUMBER
4. TITLE (and Subtitle) WHISTLER MODE TURBULENCE GENERATED BY ELECTRON BEAMS IN EARTH'S BOW SHOCK		5. TYPE OF REPORT & PERIOD COVERED Progress, May, 1983
		6. PERFORMING ORG. REPORT NUMBER
7. AUTHOR(s) R. L. TOKAR, D. A. GURNETT, and W. C. FELDMAN		8. CONTRACT OR GRANT NUMBER(s) N00014-76-C-0016
9. PERFORMING ORGANIZATION NAME AND ADDRESS Department of Physics and Astronomy The University of Iowa Iowa City, IA 52242		10. PROGRAM ELEMENT, PROJECT, TASK AREA & WORK UNIT NUMBERS
11. CONTROLLING OFFICE NAME AND ADDRESS Office of Naval Research Electronics Program Office Arlington, VA 22217		12. REPORT DATE May, 1983
		13. NUMBER OF PAGES 47
14. MONITORING AGENCY NAME & ADDRESS(If different from Controlling Office)		15. SECURITY CLASS. (of this report) UNCLASSIFIED
		15a. DECLASSIFICATION/DOWNGRADING SCHEDULE

16. DISTRIBUTION STATEMENT (of this Report)

Approved for public release; distribution is unlimited.

17. DISTRIBUTION STATEMENT (of the abstract entered in Block 20, if different from Report)

18. SUPPLEMENTARY NOTES

19. KEY WORDS (Continue on reverse side if necessary and identify by block number)

Bow shock, Whistler Mode Waves

20. ABSTRACT (Continue on reverse side if necessary and identify by block number)

(See page following)

DD FORM 1473 EDITION OF 1 NOV 65 IS OBSOLETE
1 JAN 73
S/N 0102-LF-014-6601

ABSTRACT

In this study, the Landau and cyclotron growth rates of whistler mode waves in Earth's bow shock are calculated using electron distribution functions obtained with the fast plasma experiment on ISEE 2. Three electron distribution functions measured within the transition region of the shock are analyzed. An important feature of these electron distribution functions is the presence of a field-aligned beam with a $(T_\perp) > (T_\parallel)$ anisotropy. The beam velocity vector is directed toward the magnetosheath. The calculations show that the electron distribution functions spontaneously generate whistler mode waves with plasma rest frame frequencies between about .1 and 100 Hz. The wave normal angles of the generated whistlers range from 0° to the resonance cone angle. Electromagnetic Landau resonance and/or cyclotron resonance contribute to wave growth over the range of velocity distributions observed. The waves that are generated by the normal cyclotron resonance have wave vectors directed toward the solar wind while those that are generated by the Landau and the anomalous cyclotron resonances have wave vectors directed toward the magnetosheath. The predictions of the study are in qualitative agreement with observations of whistler mode waves near Earth's bow shock.

I. INTRODUCTION

Although shock waves in collisionless plasmas have been studied
for more than two decades, the physics of collisionless shocks is still
not well understood. Much of the current theoretical effort is aimed
at formulating models that self-consistently describe the observed
shock structures and the shock dissipation mechanisms. In a collision-
less shock wave the upstream unshocked plasma is transformed into the
downstream shocked plasma within a spatial length that is smaller than
the mean free paths of the plasma particles. The region separating the
upstream and downstream plasmas within which the dissipation occurs is
called the transition region. Observations of fluctuating electric and
magnetic fields associated with shocks in the laboratory and in inter-
planetary space indicate that plasma wave turbulence plays an important
role in electron and ion heating at the shock. For information and
additional references on the subject of both natural and laboratory
shock waves, the interested reader can refer to Tidman and Krall
[1971], Biskamp [1973], Galeev [1976], Formisano [1977], and Greenstadt
and Fredericks [1979].

Earth's bow shock, the shock wave formed by the interaction of the
solar wind with Earth's magnetic field, provides an excellent labora-
tory for the study of collisionless shock waves. The characteristics
of the bow shock are highly variable because the parameters that

characterize the upstream solar wind vary over a broad range. In addition, because spacecraft instruments have dimensions smaller than characteristic shock scale lengths, the shock fine structure can be studied in detail if high time resolution instrumentation is used or if the spacecraft is moving slowly with respect to the shock.

Among the experiments on board the ISEE 1 and 2 satellites are a fast plasma experiment [Bame et al., 1978] and a plasma wave experiment [Gurnett et al., 1978]. The fast plasma experiment is specifically designed to measure distribution functions in one dimension in approximately 100 milliseconds and distribution functions in two dimensions in one spin period (3 seconds). In particular, the time resolution of the fast plasma experiment is sufficient to allow the measurement of distinctive features of electron distribution functions within the shock transition region with negligible aliasing of time. An important new feature of the electron distribution functions measured by the fast plasma experiment within the shock transition region is a field-aligned beam moving toward the magnetosheath [Feldman et al., 1982; 1983]. The beam is observed for both quasi-parallel and quasi-perpendicular turbulent shocks. Quasi-parallel and quasi-perpendicular refer to the angle between the shock normal and the ambient magnetic field, θ_{Bn}. For a quasi-parallel shock, θ_{Bn} is greater than 0° but less than about 45° while for a quasi-perpendicular shock θ_{Bn} is greater than about 45° but less than 90°.

The plasma wave experiment observes many types of plasma turbulence in association with Earth's bow shock. This turbulence is similar to the plasma waves observed near the bow shock by previous

instrumentation [Fredericks et al., 1968; Rodriguez and Gurnett, 1975].
Among the different types of electrostatic and electromagnetic waves
observed is whistler mode turbulence. Whistler mode waves are electro-
magnetic waves that propagate at frequencies below either the electron
gyrofrequency, ω_g, or the electron plasma frequency, ω_p. In the solar
wind and bow shock regions, ω_g is always much less than ω_p. Typically,
the whistler mode noise is most intense within the shock transition
region and is observed to extend short distances into the upstream
solar wind and much longer distances into the downstream magnetosheath.

The purpose of this study is to demonstrate that the electron
beams measured by the ISEE 2 fast plasma experiment in the transition
region of the bow shock can generate whistler mode instabilities. The
generation mechanisms are identified and the subsequent propagation of
the whistler mode waves are discussed.

In addition to data obtained with the fast plasma experiment and
the plasma wave experiment, the study also makes use of data obtained
with the ISEE 1 and 2 magnetic field experiment [Russell, 1978].

II. TRANSITION REGION ELECTRON DISTRIBUTION FUNCTIONS

The electron distribution functions analyzed in this study were measured by the fast plasma experiment within the transition region of Earth's bow shock. In many instances, it is possible to fit the data obtained by the fast plasma experiment to simple analytic functions. Because the measurement of and fitting procedure for these electron distribution functions is described in detail in the recent reports of Feldman et al. [1982, 1983], only a brief summary will be given here.

In Figure 1, slices of electron distribution functions measured along the direction of the magnetic field on December 13, 1977, by the ISEE 2 fast plasma experiment are shown. This figure is reproduced from Feldman et al. [1982]. The figure depicts parallel slices in the solar wind (SW), the shock transition region, and the magnetosheath (MS). Data for the full two-dimensional electron distribution function obtained with the fast plasma experiment suggests that the solar wind electron distribution function is a nearly isotropic Maxwellian at this time and that the magnetosheath electron distribution function is a nearly isotropic modified Lorentzian at this time. As the satellite enters the shock transition region, field-aligned electron beams are observed. The beams are moving toward the magnetosheath and the beam velocity increases with increasing shock penetration. This figure supports the fact that the electron distribution functions measured in

the shock transition region have both a flat-topped component and a beam component.

The analytic representation of the electron distribution function in the plasma rest frame, $F(v_\perp, v_\parallel)$, is constructed from two measurements of the electron distribution function in planes parallel ($v_\parallel$) and perpendicular ($v_\perp$) to the ambient magnetic field separated in time by about 0.75 sec. Measurements of the electron distribution function in planes other than those parallel and perpendicular to the magnetic field confirm that the fits to these two data sets yield, for the purposes of this study, a sufficiently accurate representation of $F(v_\perp, v_\parallel)$. The simple analytic function used to fit the data is a sum of a convected Maxwellian and a modified Lorentzian. The convected Maxwellian models the electron beam and the modified Lorentzian models the flat-topped component of the electron distribution function. These models provide excellent fits to both the parallel and the perpendicular slices of the distribution function.

Specifically, $F(v_\perp, v_\parallel)$ is given by

$$F(v_\perp, v_\parallel) = F_1 + F_2$$

where

$$F_1 = \frac{C_1}{\left(1 + \left(\frac{(v_\parallel - v_1)^2 + v_\perp^2}{v_2^2}\right)^R\right)^{P/R}}$$

is the modified Lorentzian and

$$F_2 = C_2 \exp\left(\frac{-m(v_\parallel - v_3)^2}{2\kappa T_\parallel}\right) \exp\left(\frac{-m\, v_\perp^2}{2\kappa T_\perp}\right)$$

is the convected Maxwellian. In these equations, P and R are real numbers, $T_\perp$ and $T_\parallel$ are perpendicular and parallel temperatures, m is the electron mass, κ is Boltzman's constant, and C_1, C_2, v_1, v_2 and v_3 are constants.

It should be noted that for the electron distribution functions analyzed in this study, the direction of positive $v_\parallel$, be it parallel or anti-parallel to the magnetic field, is determined by the bow shock geometry at the observation time. The positive $v_\parallel$ direction is defined to be such that $\hat{v}_\parallel \cdot \hat{n}$ is positive, where $\hat{v}_\parallel$ is a unit vector in the positive $v_\parallel$ direction and $\hat{n}$ is a unit vector in the direction of the shock normal and toward the solar wind. Consequently, because the beam velocity vectors are always directed toward the magnetosheath, the convection speed, v_3, is always negative.

The magnitude of the beam convection speed increases with increasing shock penetration. This variation is consistent with the interpretation that the beams represent solar wind electrons that are accelerated by a macroscopic electric field within the shock transition region. The parallel temperature of the beam, $T_\parallel$, is obtained from the fit to the fast plasma experiment data. However, in many cases the corresponding perpendicular beam temperature, $T_\perp$, changes significantly

during the time it takes for the detector to rotate from the parallel
to the perpendicular orientations. Consequently, $T_\perp$ is estimated
assuming that the first adiabatic invariant of the electrons is con-
served as the electrons move from the solar wind into the shock. When
the relative motion between the spacecraft and the bow shock suffi-
ciently slow so that $T_\perp$ can be obtained, the calculated and n ured
perpendicular beam temperatures are in good agreement.

In this study, three electron distribution functions mea   by
the ISEE 2 fast plasma experiment within the transition region of
Earth's bow shock are analyzed. Of the three, two were measured on
December 13, 1977, and one was measured on October 15, 1978. The two
electron distribution functions obtained in the transition region
on December 13, 1977, correspond closely to the distributions measured
at 17:34:55.8 and 17:34:58.6 that are depicted in Figure 1. The
October 15, 1978, electron distribution function is included in this
study because the magnitude of the convection speed of the Maxwellian
modelling the electron beam is particularly small, which leads to some-
what different instability conditions than for the December 13 cases.

In Figure 2, contour plots of the best-fitting analytic models for
the three electron distribution functions analyzed in this study are
shown. Plotted are contours of constant $\log_{10} F(v_\perp, v_\parallel)$ spanning one
order of magnitude of F. The convected Maxwellians with $T_\perp > T_\parallel$
anisotropies that model the electron beams are clearly visible as is
the flat-topped feature of the modified Lorentzians. In Table 1, the
constants used to specify these three electron distribution functions

are given. In Table 2, the bow shock parameters at the three observation times are summarized. For both shock crossings, the bow shock classification is turbulent.

III. METHOD OF CALCULATING THE GROWTH RATE

To calculate the growth rate of whistler mode waves, the results obtained by Kennel and Wong [1967] using the linearized Vlasov and Maxwell equations are employed. The expression used is equivalent to the results given by Kennel [1966]. If Landau and first order cyclotron resonance terms are included and ion motion is neglected, the growth rate, ω_i, is given by

$$\omega_i = |\omega_r| \, \text{sign}\left(\frac{\omega_r}{k_\parallel}\right) \frac{\omega_p^2}{\omega_r^2} \frac{\pi}{16} \int_0^\infty v_\perp^2 (I_{-1} + I_o + I_1) dv_\perp \qquad (1)$$

where

$$I_m = \frac{(\epsilon_L J_{m-1}(x) + \epsilon_R J_{m+1}(x) - \sqrt{2}\left(\frac{v_\parallel}{v_\perp}\right)\epsilon_\parallel J_m(x))^2 (v_\perp \frac{\partial F}{\partial v_\parallel} - \frac{m\omega_g}{k_\parallel} \frac{\partial F}{\partial v_\perp})}{W} \Bigg|_{v_\parallel = \frac{\omega_r + m\omega_g}{k_\parallel}}$$

and W, the total wave energy, is given by

$$W(\vec{k},\omega) = \frac{1}{16\pi} [\vec{B}^*(\vec{k},\omega)\cdot\vec{B}(\vec{k},\omega) + \vec{E}^*(\vec{k},\omega)\cdot(\frac{\partial}{\partial\omega}\omega\vec{K}^h)\cdot\vec{E}(\vec{k},\omega)]$$

In these equations, F is the electron distribution function normalized to unity, ω_r is the real frequency of the wave, k is the wave number, ϵ_L, ϵ_R, and $\epsilon_\parallel$ are the left-hand, right-hand, and parallel electric field polarization vectors of the wave, $\overleftrightarrow{K}^h$ is the Hermitian part of the dielectric tensor, ω_g is the absolute value of the electron gyro-frequency, and x is $\dfrac{k_\perp v_\perp}{\omega_g}$. The Landau contribution to the growth rate is the m = 0 term and the normal and anomalous cyclotron resonance contributions are given by the m = -1 and the m = +1 terms. A positive growth rate indicates exponential growth and a negative growth rate indicates exponential damping.

In order to employ Equation 1 to calculate growth rates for whistler mode waves, the real part of the whistler mode dispersion relation must be solved for ω_r as a function of k. For simplicity, this study assumes that the real part of the whistler mode dispersion relation is that of a cold plasma. When the wave phase velocity is much greater than the electron thermal speed, hot plasma effects on dispersion for the whistler mode are small (e.g., see Leimohn [1962]). However, in the work reported here the wave phase velocities are often comparable to the electron thermal velocities. To investigate the error introduced by this simplifying assumption, the numerical code of Forslund [1979], which solves the fully electromagnetic linear dispersion relation, has been utilized to determine the real frequency, ω_r, for a given wave number, k [S. P. Gary, private communication]. For parameters typical of this study, the results indicate that for a given wave number and for wave normal angles $\theta \lesssim 45°$, where the wave normal

angle is the angle between the wave vector and the magnetic field, the real frequency for a cold plasma and the real frequency obtained using the code of Forslund differ by not more than 30 percent. If k is held constant and ω_r is allowed to vary by 30 percent, the computations show that the change in the growth rate calculated using Equation 1 is, for the majority of unstable wave numbers, small. As the wave normal angle approaches the resonance cone angle, $\theta_{Res} \approx \cos^{-1}(\frac{\omega_r}{\omega_g})$, the index of refraction becomes infinite and the wave becomes predominantly electrostatic. For wave normal angles near the resonance cone angle, the difference between the real frequency for a cold plasma and the real frequency obtained using the code of Forslund for a given k is larger than it is for small wave normal angles. Consequently, it should be noted that while the primary results of this study are not affected by the simplifying assumption used in calculating the growth rate, the calculated growth rates for wave normal angles near θ_{Res} are not accurate.

IV. GROWTH RATE CALCULATIONS AND GENERATION MECHANISMS

Growth rates for whistler mode waves have been calculated using Equation 1 and the electron distribution functions depicted in Figure 2. The results indicate that these electron distribution functions are unstable to whistler mode waves. In this section, the growth mechanisms that generate the whistler mode waves are discussed.

From Equation 1 it is observed that the total growth rate is a sum of three terms: the two cyclotron resonance contributions and the Landau resonance contribution. The sign of the growth rate is positive if the sum of the three contributions is positive. The signs of the $m = -1$, 0, and $+1$ contributions are positive or negative depending on whether or not the following quantity is positive or negative:

$$
\text{sign}(\frac{\omega_r}{k_\parallel}) \int_0^\infty (v_\perp \frac{\partial F}{\partial v_\parallel} - \frac{m\omega_g}{k_\parallel} \frac{\partial F}{\partial v_\perp}) \Bigg|_{v_\parallel = \frac{\omega_r + m\omega_g}{k_\parallel}} v_\perp^2 dv_\perp \tag{2}
$$

which can be rewritten in the form

$$\text{sign}(\frac{\omega_r}{k_\parallel}) \int_0^\infty (v_\perp \frac{\partial F}{\partial v_\parallel} + (\frac{\omega_r}{k_\parallel} - v_\parallel)\frac{\partial F}{\partial v_\perp} \bigg| \ v_\perp^2 dv_\perp \qquad . \qquad (3)$$

$$v_\parallel = \frac{\omega_r + m\omega_g}{k_\parallel}$$

Integrating the second term in Equation 3 by parts and introducing the electron pitch angle, α, where α is measured from the positive $v_\parallel$ axis, Equation 3 can be rewritten as

$$\text{sign}(\frac{\omega_r}{k_\parallel}) \ [-\frac{2\omega_r}{k_\parallel} \int_0^\infty Fv_\perp dv_\perp - \int_0^\infty \frac{\partial F}{\partial \alpha} v_\perp^2 dv_\perp] \bigg|_{v_\parallel = \frac{\omega_r + m\omega_g}{k_\parallel}} \qquad . \qquad (4)$$

The whistler mode waves generated in the transition region by the electron distribution functions shown in Figure 2 fall naturally into two categories: waves with wave vectors predominantly in the opposite direction of the beam velocity and waves with wave vectors predominantly in the direction of the beam velocity. For waves propagating in the direction opposite to the beam, i.e., toward the solar wind, $k_\parallel$ is positive and the growth mechanism is the normal $m = -1$ cyclotron resonance. All three electron distribution functions shown in Figure 2 generate whistler mode waves via the $m = -1$ cyclotron resonance. For waves propagating in the direction of the beam, i.e., toward the magnetosheath, $k_\parallel$ is negative and the growth mechanisms are the $m = 0$ Landau and the anomalous $m = +1$ cyclotron resonance. Of the three electron distribution functions shown in Figure 2, only the

distribution function measured on October 15, 1978, generates whistler

mode waves propagating in the direction of the beam. In the following

subsections, the cases $k_\parallel > 0$ and $k_\parallel < 0$ are examined.

A. Wave Vectors Directed Toward the Solar Wind: Generation Via the m = -1 Resonance

To investigate the generation of whistler mode waves by the normal

m = -1 cyclotron resonance contribution to the growth rate, consider

Equations 2 through 4 when m = -1. Because the beams depicted in Figure

2 are moving in the direction of the magnetosheath, the parallel compo-

nent of the wave vector must be positive for interactions via the m = -1

cyclotron resonance. For the distribution functions shown in Figure 2,

the second term in Equation 2 is negative. Therefore, in order for

Equation 2 to be positive, $v_\perp^3 \frac{\partial F}{\partial v_\parallel}$ evaluated at the m = -1 cyclotron

resonance velocity, $v_\parallel = \frac{\omega_r - \omega_g}{k_\parallel}$, and integrated over all $v_\perp$ must be

sufficiently positive to overcome the negative term. Equivalently, Equa-

tion 4 expresses the result that a region of sufficiently large

anisotropy, $\frac{\partial F}{\partial \alpha} < 0$, along the m = -1 cyclotron resonance velocity must

exist if the growth rate is to be positive.

From these facts it is expected that the electron distribution

functions shown in Figure 2 will generate whistler mode waves if the

cyclotron resonance velocity has a larger magnitude than the magnitude

of the convection speed of the Maxwellian modelling the electron beam,

$|v_3|$. In this region of the electron distribution functions shown in

Figure 2, $\frac{\partial F}{\partial v_\parallel}$ is positive and $\frac{\partial F}{\partial \alpha}$ is negative.

The left column of Figure 3 shows representative growth rates obtained using the electron distribution function measured within the shock transition region at 1734:55.7 on December 13, 1977. At this time, $\frac{\omega_g}{2\pi}$ is about 315 Hz and $\frac{\omega_p}{2\pi}$ is about 20 kHz. Plotted are the ratios of total growth rate, ω_i, to real frequency, ω_r, as a function of the wave normal angle. The growth rates for the two frequencies $\omega_r/2\pi$ = 110, and 120 Hz are given. This figure depicts whistler mode waves with positive growth rates. The absence of a plotted growth rate indicates damping. For the frequencies shown here, both the m = +1 cyclotron resonance contribution to ω_i and the m = 0 Landau resonance contribution to ω_i are negative and small compared to the positive contribution of the m = -1 cyclotron resonance. The left column of Figure 3 indicates that as the frequency is increased the range of unstable wave normal angles decreases while the centroids of these angles, which range from 0 to about 80 degrees, increase. This trend can be understood from a plot of the m = -1 cyclotron resonance velocity.

The right column of Figure 3 shows the m = -1 cyclotron resonance velocity as a function of wave normal angle for the two frequencies $\frac{\omega_r}{2\pi}$ = 110 and 120 Hz. For the electron distribution function measured at 1734:55.7 on December 13, 1977, the Maxwellian modelling the electron beam is convected into the shock at a speed of about 3255 km/s. It is expected that the resonance velocity must have a larger negative value than -3255 km/s if instability is to occur as only then will $\partial F/\partial \alpha$ be

sufficiently negative (or $\partial F/\partial v_{\parallel}$ sufficiently positive) along the inte-

gration path. This point is illustrated in Figure 4 where the reso-

nance velocity range giving rise to instability for the case $\frac{\omega_r}{2\pi} = 110$ Hz,

as obtained from Figure 3, is overlayed on a contour plot of the elec-

tron distribution function measured at 1734:55.7 on December 13, 1977.

The resonance velocity lies in a region of positive $\frac{\partial F}{\partial v_{\parallel}}$ and large

anisotropy, $\frac{\partial F}{\partial \alpha} < 0$.

B. Wave Vectors Directed Toward the Magnetosheath: Generation Via the m = 0 and +1 Resonances

To investigate the generation of whistler mode waves by the m = 0

Landau and the m = +1 anomalous cyclotron resonances, Equations 2

through 4 are again examined. Because the convection speeds for the

electron beams shown in Figure 2 are negative, for the generation of

whistler mode waves via the m = 0 and the m = +1 interactions $k_{\parallel}$ is nega-

tive, corresponding to wave vectors directed toward the magnetosheath.

From Equation 2 it is seen that in order for the m = 0 Landau con-

tribution to ω_i to be positive, $-v_{\perp}^3 \frac{\partial F}{\partial v_{\parallel}}$ evaluated at the Landau reso-

nance velocity, $v_{\parallel} = \frac{\omega_r}{k_{\parallel}}$, and integrated over all $v_{\perp}$ must be positive.

Taking into account the sign of $k_{\parallel}$ with the expression $\frac{k_{\parallel}}{|k_{\parallel}|}$, this will

occur when regions of large positive $\frac{k_{\parallel}}{|k_{\parallel}|} \frac{\partial F}{\partial v_{\parallel}}$ exist along the

integration path. Considering the m = +1 cyclotron term for the case

when $k_{\parallel}$ is negative, the first term in Equation 4 is negative. Conse-

quently, the m = +1 cyclotron resonance contribution to the growth rate

will be be positive when regions of large anisotropy, $\frac{\partial F}{\partial \alpha} > 0$, exist

along the integration path.

Of the three electron distribution functions shown in Figure 2,

only the distribution function measured on October 15, 1978, generates

whistler mode waves via the m = 0 and the m = +1 resonances. This is

because the convection speeds for the electron beams in the distribution

functions measured on December 13, 1977, are large. Because the convec-

tion speeds are large, $\frac{\partial F}{\partial v_{\parallel}}$ is near zero at typical Landau resonance

veloci:ies and the Landau contribution to the growth rate is small.

Consequently, the m = -1 cyclotron contribution to damping dominates any

positive contribution to the growth rate due to the m = +1 cyclotron

resonance. This is not the case for the electron distribution function

measured on October 15, 1978, which has a smaller beam velocity.

Because the beam velocity is small, the m = 0 Landau contribution to ω_i

is large and positive.

The left column of Figure 5 presents a sample of the growth rates

obtained using the October 15, 1978, electron distribution function.

The results are given for one frequency, $\frac{\omega_r}{2\pi} = 80$ Hz. At this time, $\frac{\omega_g}{2\pi}$

is about 110 Hz and $\frac{\omega_p}{2\pi}$ is about 20 kHz. The top left panel shows the

m = 0 Landau resonance contribution to the ratio $\frac{\omega_i}{\omega_r}$ while the bottom

left panel gives the m = +1 cyclotron resonance contribution to $\frac{\omega_i}{\omega_r}$.

The m = -1 cyclotron resonance contribution to $\frac{\omega_i}{\omega_r}$ is negative and

negligible for these wave normal angles and this frequency. The right

column of Figure 5 depicts the Landau resonance velocity and the m = +1

cyclotron resonance velocity as a function of wave normal angle for

$\frac{\omega_r}{2\pi} = 80$ Hz.

From Figure 5 it is observed that the Landau contribution to ω_i is a maximum at an intermediate wave normal angle and decreases to zero at $0°$ and θ_{Res} ($\theta_{Res} \approx 43°$ here). The contribution is positive over a wide range of wave normal angles because the Landau resonance velocity lies in a region of positive $\dfrac{k_{\parallel}}{|k_{\parallel}|} \dfrac{\partial F}{\partial v_{\parallel}}$ over a wide range of wave normal angles. The Landau growth rate goes to zero at $0°$ because the whistler mode wave is purely transverse at that angle and goes to zero at θ_{Res} because the index of refraction for the whistler mode becomes very large near θ_{Res}, thereby moving the resonance velocity out of the region of large positive $\dfrac{k_{\parallel}}{|k_{\parallel}|} \dfrac{\partial F}{\partial v_{\parallel}}$.

The $m = +1$ cyclotron resonance contribution to ω_i is positive for wave normal angles between about $10°$ and $42°$. The $m = +1$ contribution falls to zero as the wave normal angle approaches $0°$ because L_{+1} in Equation 1 is identically zero at $0°$. This corresponds to the fact that a parallel propagating whistler mode wave is right-hand polarized with respect to the magnetic field, whereas the anomalous $m = +1$ resonance requires a left-hand polarization component for a resonant interaction to occur. The $m = +1$ contribution is zero for wave normal angles greater than about $42°$ because the $m = +1$ cyclotron resonance velocity does not lie in a region of sufficiently positive $\dfrac{\partial F}{\partial \alpha}$ for wave normal angles greater than $42°$.

In Figure 6, the range of unstable resonance velocities for the $m = 0$ and the $m = +1$ resonances, as obtained from Figure 5, is overlayed on a contour plot of the October 15, 1978, electron distribution function. The Landau resonance velocity lies in a region of positive

$$\frac{k_\parallel}{|k_\parallel|}\frac{\partial F}{\partial v_\parallel}$$ while the m = +1 cyclotron resonance velocity lies in regions of large anisotropy, $\frac{\partial F}{\partial \alpha} > 0$.

Figures 7 and 8 summarize the unstable frequencies and wave normal angles for the electron distribution functions shown in Figure 2. Figure 7 depicts the waves that are generated by the m = 0 and +1 resonances for the October 15, 1978, velocity distribution. The unstable region is indicated by the shading. These waves have $k_\parallel < 0$, corresponding to wave vectors directed toward the magnetosheath. The unstable frequencies and wave normal angles for generation via the m = -1 resonance are shown in Figure 8. In the bottom panel, the results for the October 15, 1978, distribution are shown while the top panels correspond to the two December 13, 1977, distributions. These whistler mode waves are all generated by the m = -1 cyclotron resonance term and have $k_\parallel > 0$.

It is desirable to identify the growth rates that are large enough to produce a rapid increase in the intensity of whistler mode noise at Earth's bow shock. To do so, the critical growth rate, ω_c, required to produce large growth over a small distance is calculated. For simplicity, the critical growth rate is defined to be the growth rate necessary for an order of magnitude increase in the amplitudes of the wave electric and magnetic fields over a distance of 100 km. An order of magnitude increase in the intensity of whistler mode noise at Earth's bow shock is consistent with plasma wave observations (e.g., see Rodriguez and Gurnett [1975]). The spatial length over which the growth occurs, 100 km, is in agreement with bow shock scale lengths obtained by Russell [1979].

To calculate the critical growth rate, the effect of the solar wind flow on the propagation of a whistler mode wave packet must be taken into account. This is because the solar wind speed is often comparable to the whistler mode group speed. Because only a rough estimate of the critical growth rate is desired, two extreme situations are considered: wave packets with group velocities in the direction of the solar wind flow and wave packets with group velocities in the opposite direction of the solar wind flow. The critical growth rates for these two cases are given by

$$\omega_c(k_\parallel < 0) = \frac{\ln 10}{L} (v_g + v_{sw}) \tag{5}$$

and

$$\omega_c(k_\parallel > 0) = \frac{\ln 10}{L} (v_g - v_{sw}) \quad . \tag{6}$$

In these equations, v_g is the whistler mode group speed, v_{sw} is the solar wind speed, and L = 100 km is the characteristic scale length of the transition region. The group speed is calculated using

$$v_g = \frac{2c \, \omega_r^{1/2} (\omega_g \cos \theta - \omega_r)^{3/2}}{\omega_p \, \omega_g \cos \theta} \tag{7}$$

where c is the speed of light and θ is the wave normal angle. The solar

wind speed is taken to have the constant value 400 km/s.

Equations 5 and 6 are used to calculate the critical growth rate for

waves with wave vectors directed toward the magnetosheath, $k_\parallel < 0$, and

for waves with wave vectors directed toward the solar wind, $k_\parallel > 0$. The

results obtained are summarized in Figures 7 and 8. The region contained

inside the dashed line in Figure 7 defines the frequencies and wave

normal angles that have a growth rate, ω_i, greater than the critical

growth rate, $\omega_c(k_\parallel < 0)$. For wave vectors directed toward the magneto-

sheath, $k_\parallel < 0$, waves with frequencies between about 5 and 85 degrees and

with intermediate wave normal angles have the largest growth rates. For

wave vectors directed toward the solar wind, $k_\parallel > 0$, Figure 8 illustrates

that nearly all of the growth rates for the velocity distributions

measured on October 15, 1978, and at 1734:55.7 on December 13, 1977, are

large. However, the distribution obtained at 1734:58.5 on December 13,

1977, does not contain enough free energy to produce growth rates larger

than the critical growth rate. At this time it is not known whether or

not this is a common feature of velocity distributions that are measured

at large shock penetration lengths.

It should be noted that the calculated growth rates are sometimes so

large that the condition $\omega_i/\omega_r \ll 1$ is not satisfied. When this condi-

tion is not met, the growth rate calculated using Equation 1 is not

accurate. It is expected that a more exact calculation of the growth

rate would yield a smaller positive value. While this difficulty does

point out the fact that some of the growth rates presented in this paper

are rough estimates, the signs of the calculated growth rates are

accurate.

V. DISCUSSION

This study has shown that electron distribution functions measured using the fast plasma experiment on ISEE 2 within the transition region of Earth's bow shock are unstable to a large spectrum of whistler mode waves. The unstable whistler mode waves have plasma rest frame frequencies between about .1 and 100 Hz and have wave vector directions with respect to the magnetic field which range from $0°$ to the resonance cone angle. In general, the lower frequency (.1 to 10 Hz) waves have wavelengths between about 500 and 100 km, while the higher frequency waves (10 to 100 Hz) have wavelengths between about 100 and 20 km. The whistler mode waves are generated by either electromagnetic Landau resonance or electromagnetic cyclotron resonance or both. The free energy regions in the electron distribution functions are regions of positive $\frac{k_{\parallel}}{|k_{\parallel}|} \frac{\partial F}{\partial v_{\parallel}}$ and regions of $T_{\perp} > T_{\parallel}$ anisotropy, both attributable to the field-aligned electron beam. If it is assumed that a background continuum of whistler mode noise is available in the solar wind for amplification, as indicated by the measurements of Neubauer et al. [1977], the stability calculations indicate that many of the unstable frequencies and wave normal angles have growth rates large enough to give rise to large whistler mode intensities at Earth's bow shock.

To fully evaluate the growth of whistler mode noise in the bow shock, it is necessary to compute the growth integrated along typical ray paths through the shock. However, a detailed treatment of this

problem is difficult because the magnetic field geometry within the transition region of Earth's bow shock is complicated. To obtain a qualitative understanding of the subsequent propagation of the generated whistler mode waves, a simple model for the shock geometry is adopted. The model is that of a parallel shock with the upstream solar wind velocity in the opposite direction of the shock normal. The ramp in the magnetic field amplitude defines the shock transition region where the electron distribution functions shown in Figure 2 are present. The electron distribution function measured on October 15, 1978, represents the distribution function often observed near the upstream boundary of the magnetic ramp. The electron distribution functions measured on December 13, 1977, represent the distribution functions often observed within the magnetic ramp.

The waves depicted in Figure 7 are produced near the upstream boundary of the magnetic ramp by the $m = 0$ and the $m = +1$ resonances and have $k_\parallel$ in the downstream direction. Because the waves with frequencies between about 5 and 85 Hz have the largest growth rates, at the upstream shock boundary a rapid increase in whistler mode intensity over this frequency range is expected. For the parallel shock model the wave packets propagate downstream and are convected downstream by the solar wind flow. This is due to the fact that the group velocity of the whistler mode is confined to angles less than about $20°$ from the magnetic field [Helliwell, 1965]. As these wave packets move downstream, they will encounter distribution functions similar to those measured on December 13, 1977. Because the electron distribution functions measured on December 13, 1977, are stable to waves with $k_\parallel < 0$, the waves will be

damped as they move downstream. It is expected that most of these waves will not reach the magnetosheath as the damping rate can be large.

The waves depicted in Figure 8 are generated by the m = -1 cyclotron resonance and have $k_\parallel$ in the upstream direction. For the simple shock model adopted the solar wind will convect the wave packets downstream if the group speed is smaller than the solar wind speed, which has the typical value 400 km/s. For plasma parameters typical of the bow shock region and for the frequencies of interest in this study, the group speed of the whistler mode is smaller than 400 km/sec for wave normal angles near θ_{Res}. Consequently, in the simple shock model only the whistler mode waves with wave normal angles near the resonance cone angle are convected downstream by the solar wind flow. The remaining whistler mode waves either travel upstream against the solar wind flow or stand in the shock. It is possible that the standing whistlers so produced contribute to the overall shock structure because many of the standing whistlers have wavelengths equal to the shock thickness.

Because the electron distribution function measured on October 15, 1978, represents the typical distribution near the upstream shock boundary the growth rate calculations for this distribution predict which whistlers will travel into the solar wind. The calculations summarized in the bottom panel of Figure 8 suggest that low frequency ($\approx$ 7 - 30 Hz) waves travel into the upstream solar wind. A range in wave normal angles from 0° to near θ_{Res} is expected.

These predictions are summarized as follows:

1) Intense broadband whistler mode noise is generated by the m = 0, +1, and -1 resonances in the shock transition region.

2) The whistler mode noise in front of the magnetic ramp will be most prevalent at low (7 - 30 Hz) frequencies. These waves are generated by the normal, m = -1, cyclotron resonance, and have wave normal angles from 0° to near θ_{Res}.

3) At the upstream boundary of the magnetic ramp, whistler mode waves with frequencies between about .1 and 100 Hz are produced via the m = 0 and +1 resonances. The waves with frequencies between about 5 and 85 Hz have the largest growth rates. Because these waves are damped as they travel downstream, most of the waves are not expected to reach the magnetosheath.

It is desirable to compare the predictions of this study with observations of whistler mode waves near Earth's bow shock. However, because the predicted frequencies are with respect to the plasma rest frame, they are not the frequencies actually measured by a plasma wave receiver. The measured frequencies are Doppler-shifted by the relative motion of the satellite and the plasma. Simple calculations show that in most cases the measured frequency is expected to be between about one-half to two times the rest frame frequency. Because the Doppler effect at the shock is difficult to treat in detail, in this paper only a qualitative comparison of the predictions of the study and observations of whistler mode waves will be made.

In Figure 9, data obtained on December 13, 1977, by the plasma wave experiment and the magnetic field experiment on board ISEE 1 are shown. ISEE 1, as opposed to ISEE 2, data are shown because wave magnetic field measurements, which are most useful for detecting whistler mode noise, were only available from ISEE 1 for the event studied. The spatial

separation of the two satellites is small. By comparing the ISEE 1 and the ISEE 2 magnetic field profiles at these times, the temporal separation of the two data sets measured on December 13, 1977, is found to be about 15 seconds. For example, the time 1735:00.0 on ISEE 2 corresponds to 1735:15.0 on ISEE 1.

The top panel of Figure 9 shows the wave magnetic fields in ten channels covering the frequency range 5.6 Hz to 1 kHz and the time period 1730:00.0 to 1740:00.0 UT on December 13, 1977. The bottom panel depicts the magnetic field strength over the same time period. The magnetic ramp defining the shock transition region is clearly visible, with the upstream boundary at about 1735:05.0. At this time, the satellite enters the shock from the solar wind. It is assumed that the electron distribution function at the upstream boundary of the magnetic ramp is similar to the October 15, 1978, electron distribution function. Within the magnetic ramp at about 1735:20.0, the electron distribution functions are those measured by the ISEE 2 fast plasma experiment on December 13, 1977.

In Figure 9, whistler mode noise is visible in the bottom six frequency channels of the wave magnetic field data. As predicted by this study, the noise has largest intensity within the magnetic ramp. The frequency range over which the noise is observed, from about 5.6 to 100 Hz, is in good agreement with the results of this study. In the solar wind immediately upstream of the magnetic ramp, the noise is most intense at low frequencies, in agreement with prediction 2 above. This figure, which is typical of whistler mode observations at the bow shock, illustrates that the predictions of this study and the observations of whistler mode waves compare favorably.

ACKNOWLEDGEMENTS

TABLE 1

Parameters Which Specify the Electron Distribution Functions in Figure 2

DATE AND TIME (UT)	C_1 (Arbitrary Units)	C_2 (Arbitrary Units)	v_1 (km/s)	v_2 (km/s)	v_3 (km/s)	P	R	$T_\perp$ (°K)	$T_\parallel$ (°K)
10/15/78 1821:02.0	6.14×10^7	6.00×10^7	0.0	2600.0	1970.0	3.29	2.29	4.00×10^5	3.60×10^4
12/13/77 1734:55.7	2.10×10^7	1.20×10^7	0.0	3650.0	3255.0	3.43	2.43	2.70×10^5	2.00×10^4
12/13/77 1734:58.5	8.05×10^6	7.10×10^6	277.0	5250.0	5363.0	4.26	3.00	2.60×10^5	2.40×10^4

TABLE 2

Shock Parameters

DATE AND TIME (UT)	θ_{Bn} (Degrees)	Magnetic Local Time (Hours)	Radial Distance (R_E)	$\omega_p/2\pi$ (kHz)	$\omega_g/2\pi$ (Hz)
10/15/78 1821:02.0	35	12.6	14.3	20	110
12/13/77 1734:55.7	65	8.2	16.8	20	315
12/13/77 1735:00.0	65	8.2	16.8	20	315
12/13/77 1734:58.5	65	8.2	16.8	20	315

REFERENCES

Bame, S. J., J. R. Asbridge, H. E. Felthauser, J. P. Glore,
G. Paschmann, P. Hemmerich, K. Lehmann, and H. Rosenbauer, ISEE-1
and ISEE-2 fast plasma experiment and the ISEE-1 solar wind
experiment, IEEE Trans. Geosci. Electron., GE-16, 216, 1978.

Feldman, W. C., S. J. Bame, S. P. Gary, J. T. Gosling, D. McComas,
M. F. Thomsen, G. Paschmann, N. Sckopke, M. M. Hoppe, and C. T.
Russell, Electron heating within the Earth's bow shock, Phys.
Rev. Lett., 49, 199, 1982.

Feldman, W. C., R. C. Anderson, S. J. Bame, S. P. Gary, J. T. Gosling,
D. J. McComas, M. F. Thomsen, G. Paschmann, and M. M. Hoppe,
Electron velocity distributions near the Earth's bow shock,
J. Geophys. Res., 88, 96, 1983.

Formisano, V., The physics of the Earth's collisionless shock wave,
J. de Physique, 38, C6-65, 1977.

Forslund, D. W., J. M. Kindel, and M. A. Stroscio, Current driven elec-
tromagnetic ion cyclotron instability, J. Plasma Phys., 21, 127,
1979.

Fredericks, R. W., C. F. Kennel, F. L. Scarf, G. M. Crook, and I. M. Green, Detection of electric-field turbulence in the earth's bow shock, Phys. Rev. Lett., 21, 1761, 1968.

Galeev, A. A., Collisionless shocks, in Physics of Solar Planetary Environments, Vol. 1, ed. by D. J. Willians, American Geophysics Union, 1976.

Greenstadt, E. W., and R. W. Fredericks, Shock systems in collisionless space plasmas, in Solar System Plasma Physics, Vol III, ed. by C. F. Kennel, L. J. Lanzerotti, and E. N. Parker, North-Holland Publishing Company, 1979.

Greenstadt, E. N., R. W. Fredericks, C. T. Russell, F. L. Scarf, R. R. Anderson, and D. A. Gurnett, Whistler mode wave propagation in the solar wind near the bow shock, J. Geophys. Res., 86, 4511, 1981.

Gurnett, D. A., F. L. Scarf, R. W. Fredericks, and E. J. Smith, The ISEE 1 and ISEE 2 plasma wave investigation, IEEE Trans. Geosci. Electron., GE-16, 225, 1978.

Helliwell, R. A., Whistlers and related ionospheric phenomena, Stanford University Press, Stanford, California, 1965.

Kennel, C. F., Low-frequency whistler mode, Phys. of Fluids, 9, 2190, 1966.

Kennel, C. F., and H. V. Wong, *Resonant particle instabilities in a uniform magnetic field*, J. Plasma Physics, 1, 75, 1967.

Leimohn, H. B., and F. L. Scarf, Whistler attenuation by electrons with an $E^{-2.5}$ distribution, J. Geophys. Res., 67, 4163, 1962.

Neubauer, F. M., H. J. Beinroth, H. Barnstorf, and G. Dehmel, Initial results from the Helios-1 search coil magnetometer experiment, J. Geophys. Res., 42, 599, 1977.

Rodríguez, P., and D. A. Gurnett, *Electrostatic and electromagnetic turbulence associated with the Earth's bow shock*, J. Geophys. Res., 80, 19, 1975.

Russell, C. T., The ISEE-1 and -2 fluxgate magnetometers, IEEE Trans. Geosci. Electron., GE-16, 239, 1978.

Russell, C. T., and E. W. Greenstadt, Initial ISEE magnetometer results: Shock observations, Space Sci. Rev., 23, 3, 1979.

Tidman, D. A., and N. Krall, Shock Waves in Collisionless Plasmas, John Wiley-Interscience, New York, 1971.

FIGURE CAPTIONS

Figure 1   This figure, reproduced from Feldman et al. [1982],
            shows parallel slices of electron distribution func-
            tion data measured by the ISEE 2 fast plasma experi-
            ment. As the satellite moves from the solar wind
            into the magnetosheath, field-aligned electron beams
            are observed.

Figure 2   This figure depicts contour plots of the logarithm of
            the analytic fits to the electron distribution func-
            tion data analyzed in this study. These distribu-
            tion functions were measured within the transition
            region of Earth's bow shock. A modified Lorentzian
            models the flat-topped component of the electron dis-
            tribution and a convected Maxwellian with a $T_\perp > T_\parallel$
            anisotropy models the field-aligned electron beam.

Figure 3   The left column of this figure presents a sample of
            the growth rates obtained for the electron
            distribution function measured on December 13, 1977,
            at 1735:55.7. Plotted is the ratio of the total
            growth rate to real frequency. These waves are

generated by the m = -1 cyclotron resonance and have

$k_{\parallel} > 0$. The right column of this figure depicts the

m = -1 cyclotron resonance velocity as a function of

wave normal angle for the two frequencies of

interest.

Figure 4   In this figure, the range in the m = -1 cyclotron

resonance velocity corresponding to instability for

$\omega_r/2\pi$ = 110 Hz, as obtained from Figure 2, is over-

layed on a contour plot of the electron distribution

function measured on December 13, 1977, at 1734:55.7.

The m = -1 cyclotron resonance velocities lie in

regions of large anisotropy, $\frac{\partial F}{\partial \alpha} < 0$.

Figure 5   The left column of this figure presents a sample of

the growth rates obtained for the electron distribu-

tion function measured on October 15, 1978, and for

the frequency $\omega_r/2\pi$ = 80 Hz. The unstable waves have

$k_{\parallel} < 0$, corresponding to wave vectors directed toward

the magnetosheath. The top left panel shows the m = 0

Landau contribution to the growth rate while the

bottom left panel shows the m = +1 cyclotron contri-

bution to the growth rate. For this frequency and

these wave normal angles the m = -1 cyclotron contri-

bution to ω_i/ω_r are negative and negligible. The

right column depicts both the m = 0 Landau resonance

velocity and the m = +1 cyclotron resonance velocity
as a function of the wave normal angle.

Figure 6   In this figure, the range in the m = 0 Landau and the
m = +1 cyclotron resonance velocities corresponding
to instability for the case $\omega r/2\pi$ = 80 Hz, as
obtained from Figure 4, is overlayed on a contour
plot of the electron distribution function measured
on October 15, 1978.   The m = 0 Landau resonance
velocities lie in regions of positive $\frac{k_{\parallel}}{|k_{\parallel}|} \frac{\partial F}{\partial v_{\parallel}}$ while
the m = +1 cyclotron resonance velocities lie in a
region of large anisotropy, $\frac{\partial F}{\partial \alpha} > 0$.

Figure 7   This figure depicts the unstable frequencies and wave
normal angles that are generated by the m = 0 and +1
resonances for the electron distribution function
measured on October 15, 1978.   The waves have $k_{\parallel} < 0$,
corresponding to wave vectors directed toward the
magnetosheath.   The largest growth rates lie in the
shaded region bounded by the dashed line.

Figure 8   This figure depicts the unstable frequencies and wave
normal angles that are generated by the m = -1 cyclo-
tron resonance for the electron distribution functions
shown in Figure 2.   All of the waves and have $k_{\parallel} > 0$,
corresponding to wave vectors directed toward the

solar wind. The growth rates for the distribution measured at 1734:58.5 on December 13, 1977, are smaller than the critical growth rate.

Figure 9   This figure depicts data obtained with the ISEE-1 plasma wave experiment and the magnetic field experiment. The top panel shows the wave magnetic fields for six frequency channels. The bottom panel illustrates the magnetometer data. The magnetic ramp at the shock is clearly visible. The characteristics of the whistler mode noise at the shock are in good agreement with the predictions of this study.

ISEE 2   Φ=-60°   13 DEC 1977
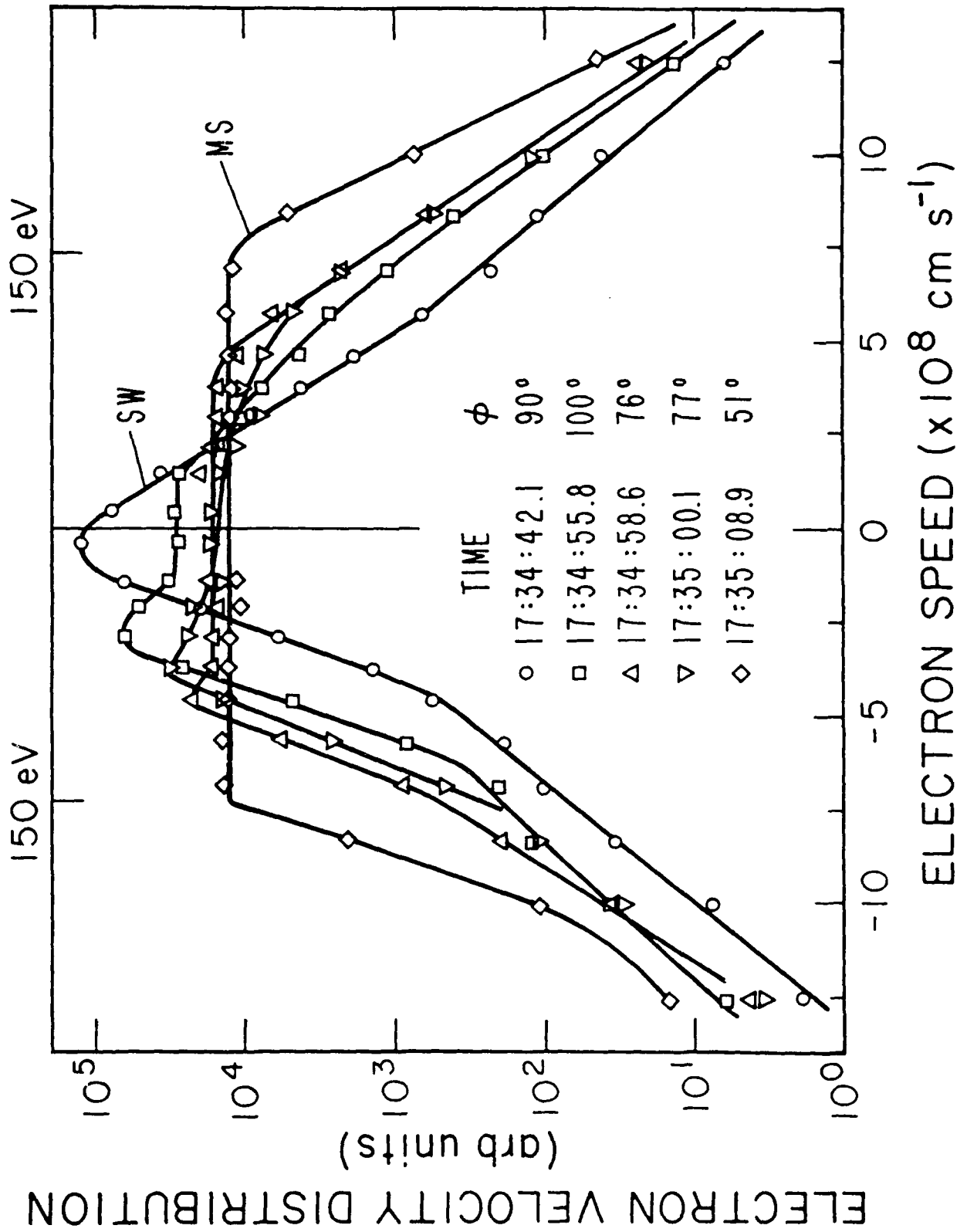
Figure 1

Figure 2

Figure 3

C-G83-8I8

DEC. 13, 1977
1734:55.7

$V_{||} = (\omega_r - \omega_g)/k_{||}$

$V_\perp$

$(\times 10^8 \text{ cm/s})$

$V_{||}$

$(\times 10^8 \text{ cm/s})$

Figure 4

Figure 5

44

Figure 6

C-G83-821

Figure 7

Figure 8

Figure 9

END